Available online at www.sciencedirect.com

ScienceDirect

Ceramics International 42 (2016) 1666–1671

CERAMICS INTERNATIONAL

www.elsevier.com/locate/ceramint

High-surface area co-electrospun TiO_2 nanowires fabricated using shrinkage of polyvinylpyrrolidone for improved photovoltaic performance

Bon-Ryul Koo, HyeLan An, Hyo-Jin Ahn*

Department of Materials Science & Engineering, Seoul National University of Science and Technology, Seoul 139-743, Republic of Korea

Received 26 August 2015; received in revised form 21 September 2015; accepted 21 September 2015
Available online 9 October 2015

Abstract

Surface-roughened TiO_2 nanowires (NWs) were fabricated using co-electrospinning with different molecular weights of polyvinylpyrrolidone (PVP) polymer: low molecular weight PVP ($M_w = 360{,}000$ g/mol) for the core region and high molecular weight PVP ($M_w = 1{,}300{,}000$ g/mol) for the shell region. Together with the formation mechanism, their surface property, morphology, crystal structure, and photovoltaic performance were studied. The results showed that the surface-roughened TiO_2 NWs had an enhanced specific surface area because of the rough NW surface compared to the pure TiO_2 NWs. As a result, the short-circuit current density (8.94 mA/cm^2) of DSSCs fabricated with the surface-roughened TiO_2 NWs is higher than that (5.88 mA/cm^2) of the pure TiO_2 NWs. Therefore, the photoconversion efficiency of the surface-roughened TiO_2 NWs exhibited a high value of ~3.63% compared to that of the pure TiO_2 NWs. This phenomenon can be explained by the enhancement of short-circuit current density by an increased dye adsorption; this is because of the increased specific surface area induced by the NW shrinkage due to the different thermal decomposition behavior of PVP depending on the different molecular weights of PVP.
© 2015 Elsevier Ltd and Techna Group S.r.l. All rights reserved.

Keywords: B.Surfaces; TiO_2; D.Electrodes; Dye-sensitized solar cells; High specific surface area

1. Introduction

Dye-sensitized solar cells (DSSCs), which have advantages such as low toxicity, low fabrication cost, and flexibility of device, have been recognized as a potential alternative to replacing conventional crystalline solar cells [1,2]. In general, DSSCs, which are photovoltaic cells based on the light-activation mechanism of a plant photosynthetic process, are composed of a working electrode (i.e., an n-type semiconductor electrode comprising TiO_2 and ZnO) with absorbed dyes, a counter electrode, and an electrolyte [1–3]. Among these, a working electrode is an important factor that directly influences the photoconversion efficiency in DSSCs. From a morphological point of view, many efforts including various nanostructures such as nanoparticles, nanowires, and nanorods have been made for improving the performance of a working electrode [2,4,5]. In particular, one-dimensional (1-D) TiO_2 nanowires are of considerable interest owing to their unique structure relative to the fast transport rate of electrons [4]. In spite of this advantage, 1-D nanowires are limited by the low amount of dye adsorption because of their low specific surface area when compared to 0-D nanoparticles. Hence, many studied have been performed in order to increase the specific surface area of 1-D TiO_2 nanowires. For example, Wang et al. reported that TiO_2 nano-branched arrays grown on fluorine-doped tin oxide (FTO) films fabricated by a two-step process of hydrothermal and chemical growth, resulted in a higher photoconversion efficiency (~3.75%) than the bare TiO_2 nanorod arrays (~1.22%) [6]. Kang et al. fabricated highly ordered TiO_2 nanotubes with large surface area using a nanoporous alumina templating method, which showed a photoconversion efficiency of ~3.5% [7]. Despite these efforts, one-pot fabrication of TiO_2 NWs with high specific

*Corresponding author. Tel.: +82 2 970 6622; fax: +82 2 973 6657.
E-mail address: hjahn@seoultech.ac.kr (H.-J. Ahn).

http://dx.doi.org/10.1016/j.ceramint.2015.09.120
0272-8842/© 2015 Elsevier Ltd and Techna Group S.r.l. All rights reserved.

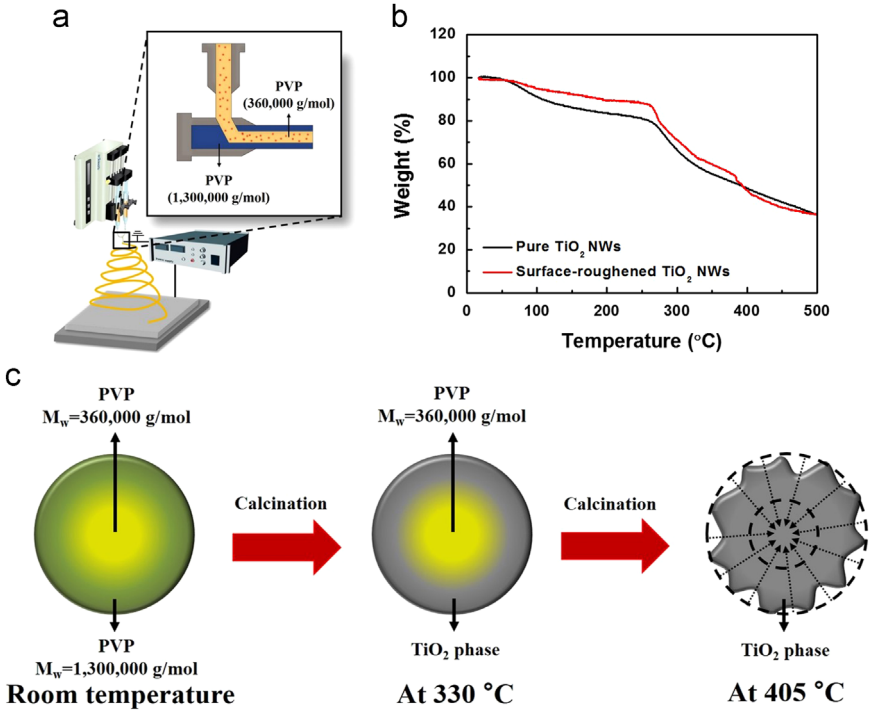

Fig. 1. A schematic illustration of a co-electrospinning apparatus (a), TGA curves obtained from the pure TiO_2 NWs and the surface-roughened TiO_2 NWs (b), and a schematic diagram of formation mechanism for the surface-roughened TiO_2 NWs by the NW shrinkage because of the different thermal decomposition behavior of PVP depending on different molecular weights (c).

surface area fabricated using co-electrospinning with different molecular weights of polyvinylpyrrolidone (PVP) has not yet been reported.

In this study, surface-roughened TiO_2 NWs having an increased specific surface area were fabricated using co-electrospinning with different molecular weights of PVP polymers. Subsequently, the relationship between their structure and photovoltaic performance as well as their formation mechanism was studied.

2. Experimental

Surface-roughened TiO_2 NWs were fabricated using co-electrospinning because of advantages such as good repeatability, low fabrication cost, simple process, and the potential for large-scale production [8,9], as shown in Fig. 1. In general, the apparatus of co-electrospinning is composed of a syringe pump, a power supply, a collector, and a needle. In particular, for co-electrospinning, two different solutions are used simultaneously using a unique needle, which is divided into two parts with core and shell regions [9]. That is, the needle of co-electrospinning has the core–shell structure with the different needle diameters which are 0.46 mm (26 gauge) for core region and 1.2 mm (18 gauge) for shell region. Therefore, the co-electrospinning is possible to selectively introduce the precursor solution in core and shell regions. In this study, titanium precursor solutions with low molecular weight PVP (M_w = 360,000 g/mol, Aldrich) in a syringe equipped with a 26 gauge needle for the core region and with high molecular weight PVP (M_w = 1,300,000 g/mol, Aldrich) in a syringe equipped with an 18 gauge needle for the shell region were prepared. The electrospinning solution was prepared by stirring titanium (IV) isopropoxide ($Ti[OCH(CH_3)_2]_4$, 97.0%, Aldrich) and acetic acid (CH_3CO_2H, 99.7%, Aldrich) in N,N-dimethylformamide (DMF, 99.0%, Aldrich) for 1 h. The weight ratio of the titanium precursor to the DMF solvent is fixed at 10 wt%. Subsequently, two different types of PVP polymers were dissolved in the above-prepared titanium precursor solution. The voltage and feeding rate were fixed at ~9.5 kV and 0.02 mL/h, respectively. The distance between the needle and collector was ~15 cm. The as-spun NWs were calcined at 500 °C to remove residues, and the surface-roughened TiO_2 NWs were finally obtained. For comparison, pure TiO_2 NWs were fabricated using single electrospinning with high molecular weight PVP.

To investigate the photovoltaic performance of DSSCs, the paste used as working electrode was prepared by dispersing the resultant TiO_2 NWs, hydroxypropyl cellulose (HCP, M_w = 80,000 g/mol, 99.0%, Aldrich), and acetylacetone ($C_5H_8O_2$, 99.0%, Aldrich) in de-ionized (DI) water. Then, the prepared TiO_2 paste was coated on FTO glass substrates (~8 Ω/square, Pilkington) using squeeze printing. After calcination at 500 °C, the TiO_2 paste-coated FTO glasses were immersed into a dye solution consisting of N719 ($Ru(dcbpy)_2(NCS)_2$, Solaronix) and ethanol (C_2H_6O, 100%, Aldrich) in a dark room for 24 h. To prepare the counter electrode, 5 mM chloroplatinic acid hexahydrate ($H_2PtCl_6 \cdot 6H_2O$, 99.9%, Aldrich) solution dissolved in 2-propanol ($(CH_3)_2CHOH$, 99.5%, Aldrich) was spin-coated onto FTO glasses, which were calcined at 450 °C for 0.5 h. Finally,

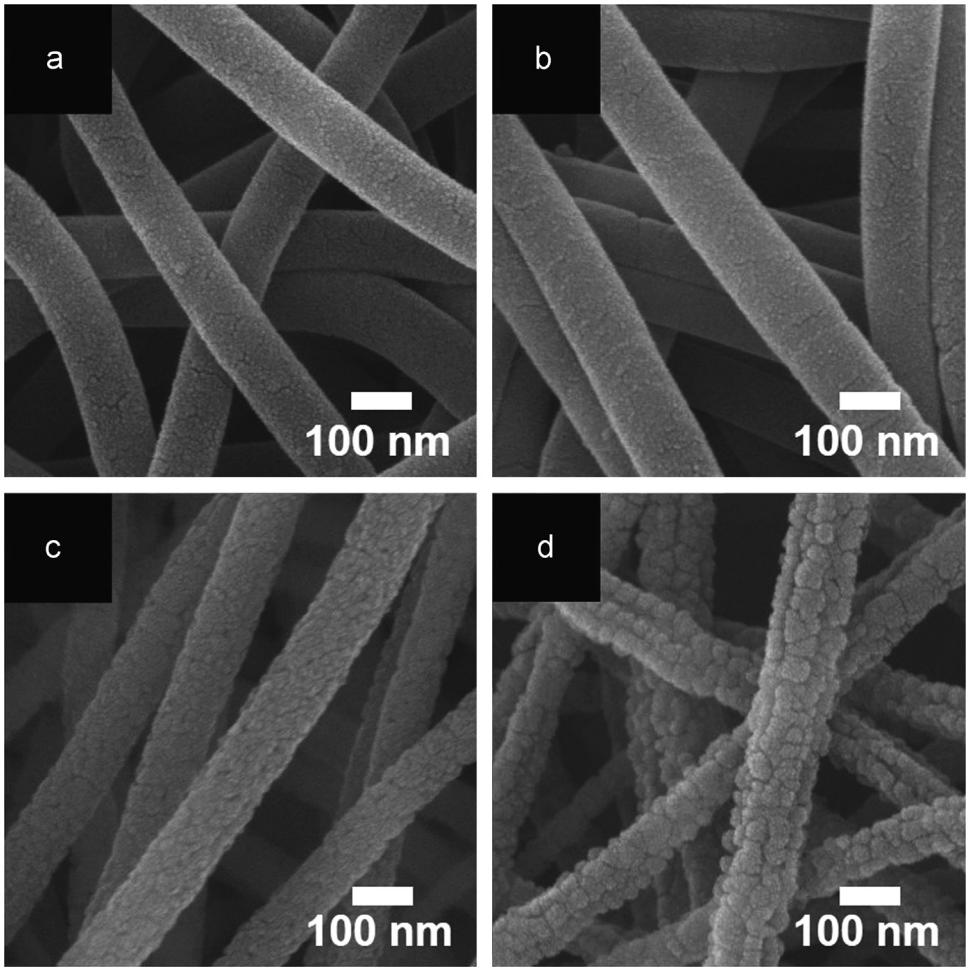

Fig. 2. FE-SEM images of the pure TiO_2 NWs and the surface-roughened TiO_2 NWs before ((a) and (b)) and after calcination ((c) and (d)).

the prepared working and counter electrodes were fabricated into sandwich-type cells. The electrolyte, a 0.6 M 1-Butyl-3-methylimidazolium iodide (BMII)-based iodine solution, was filled between the working and counter electrodes.

The weight loss of the samples was examined by thermogravimetric analysis (TGA, TGA-50, Shimadzu) over the temperature range of 15–500 °C in an air atmosphere. The morphological properties of the samples were characterized using field-emission scanning electron microscopy (FE-SEM, Hitachi S-4800) and transmission electron microscopy (MULTI/TEM, Tecnai G^2, KBSI Gwangju Center). The surface area of the two samples was measured by the Brunauer–Emmett–Teller (BET, Micromeritics ASAP2010) method. The structural properties of the samples were examined by X-ray diffraction (XRD, Rigaku X-ray diffractometer equipped with a Cu K_a radiation). The photovoltaic performance of DSSCs was evaluated using a solar simulator (McScience, K101 LAB20) with a light intensity of 100 mA/cm^2 using a 150 W xenon lamp. In order to estimate the concentration of adsorbed dyes, the dye was desorbed by immersing the working electrode into 0.1 M NaOH aqueous solution (water/ethanol = 1:1, v/v), and then analyzing the resultant solutions using ultraviolet–visible (UV–vis) spectroscopy (Perkim-Elmer Lambda-35).

3. Results and discussion

Fig. 1(a) shows the co-electrospinning apparatus for fabricating the surface-roughened TiO_2 NWs. This novel nanostructure is obtained mainly because of the unique needle types of the co-electrospinning apparatus, which is divided into core and shell regions. Using this needle type, it is possible to inject different precursor solutions at the same time, which lead to the formation of the surface-roughened TiO_2 NWs owing to the low molecular weight of PVP in the core region and the high molecular weight of PVP in the shell region. This implies that the formation mechanism of the surface-roughened TiO_2 NWs is based on the NW shrinkage because of different thermal decomposition behavior of PVP depending on different molecular weights during the calcination process. To investigate this phenomenon, TGA measurements were performed, as shown in Fig. 1(b). All the samples showed a dramatic weight loss at ~330 °C and continuous weight loss up to 500 °C, indicating the thermal decomposition of high molecular weight PVP [10]. On the other hand, the surface-

roughened TiO_2 NWs present a rapid weight loss around 405 °C, which corresponds to the thermal decomposition of low molecular weight PVP polymer [11,12]. Based on the TGA results, the formation mechanism of the surface-roughened TiO_2 NWs may be explained as shown in Fig. 1 (c). The TiO_2 phase is first formed in the shell region of the NWs because of the thermal decomposition of high molecular weight PVP around ~330 °C. When the temperature reached around 405 °C, the TiO_2 phase present in the core region started to calcine because of the different thermal decomposition of low molecular weight PVP. The successful formation of the surface-roughened TiO_2 NWs may be explained by the NW shrinkage because of the different thermal decomposition behavior of PVP depending on different molecular weights during the calcination process [13].

Fig. 2 presents the FE-SEM images obtained from the pure TiO_2 NWs and the surface-roughened TiO_2 NWs before calcination ((a) and (b)) and after calcination ((c) and (d)). All the samples before calcination are composed of a Ti precursor and a PVP, which have a uniform surface morphology. The diameters of the pure TiO_2 NWs and the surface-roughened TiO_2 NWs were in the range of ~103.3 to ~127.7 nm and ~109.2 to ~144.8 nm, respectively. In particular, the diameter difference of the samples is because of the morphology change from dense TiO_2 NWs to the surface-roughened TiO_2 NWs. After calcination, the diameter of all the samples is decreased because of thermal decomposition of the PVP when compared to the samples before calcination. Additionally, while the surface morphology of the pure TiO_2 NWs is dense, the surface-roughened TiO_2 NWs show a relatively rough surface, implying the successful formation of surface-roughened TiO_2 NWs. In order to investigate the specific surface area of the samples, BET measurements were conducted using nitrogen adsorption and desorption. The specific surface areas of the pure TiO_2 NWs and the surface-roughened TiO_2 NWs are ~23.93 m^2/g and ~67.65 m^2/g, respectively. This result indicates that the specific surface area of the surface-roughened TiO_2 NWs is 2.82-fold higher than that of the pure TiO_2 NWs, which can affect the dye adsorption on the TiO_2 NW surface in order to improve the photovoltaic performance of the DSSCs [2,14].

To further investigate the morphological properties of the TiO_2 NWs, TEM measurements were performed. Fig. 3 shows the TEM images obtained from the pure and the surface-roughened TiO_2 NWs. The nanoparticles comprising the TiO_2 NWs are between ~15.6 and ~23.0 nm for the pure TiO_2 NWs and ~14.7 and ~23.1 nm for the surface-roughened TiO_2 NWs. In particular, whereas the pure TiO_2 NWs show a uniform contrast, the surface-roughened TiO_2 NWs exhibit a relatively bright contrast in the shell region because of the successful formation of the rough NW surface.

Fig. 4 shows the XRD data obtained from the pure and surface-roughened TiO_2 NWs after calcination at 500 °C. All samples with a polycrystalline structure indicate mixed anatase and rutile TiO_2 phases. The diffraction peaks at 25.33°, 37.89°, and 48.07° correspond to the (101), (004), and (200) planes, respectively, of anatase TiO_2 (space group $I4_1/amd$ [141], JCPDS card no. 841286). Other diffraction peaks observed at 27.50°, 36.17°, 41.27°, and 55.13° correspond to the (110), (101), (111), and (211) planes, respectively, of rutile TiO_2

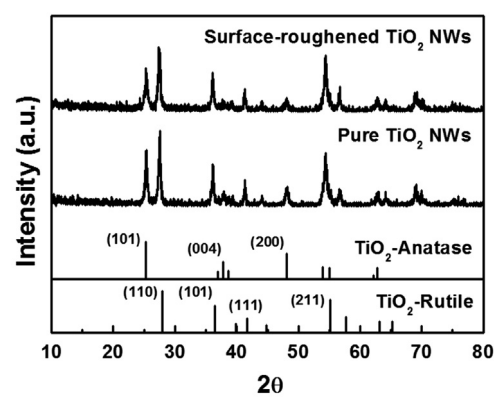

Fig. 4. XRD data of the pure TiO_2 NWs and the surface-roughened TiO_2 NWs obtained after calcination at 500 °C.

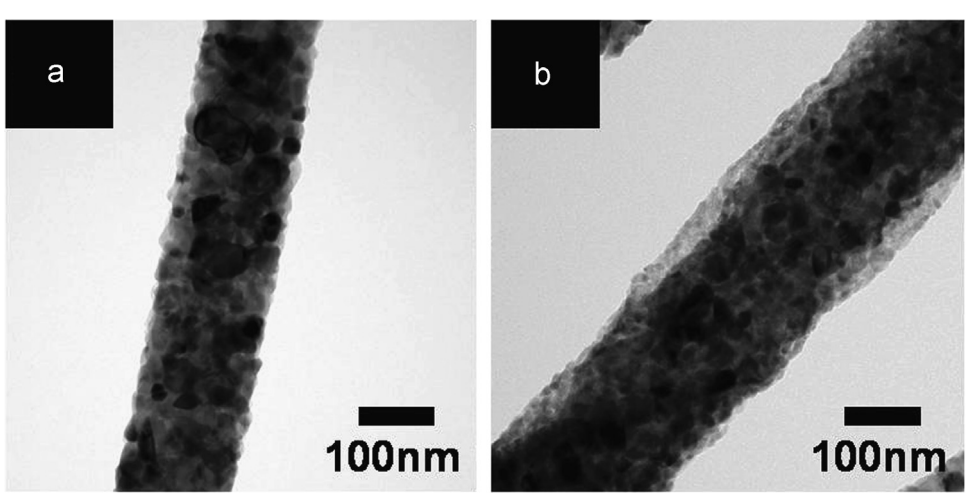

Fig. 3. TEM images obtained from the pure TiO_2 NWs (a) and the surface-roughened TiO_2 NWs (b).

(space group $P4_2/mnm$ [136], JCPDS card no. 870920). Furthermore, the difference between the peak intensities of the (101) and (110) planes indicates the relative weight percentage of the anatase and rutile phases, which can be calculated using the following equation [15]:

$$W_R = A_R/(0.884 \bullet A_A + A_R)$$

where W_R is the weight percentage of the rutile phase, A_A is the integrated intensity obtained from the (101) plane of the anatase phase, and A_R is the integrated intensity obtained from the (110) plane of the rutile phase. Therefore, the calculated weight percentage of the rutile phase was ~62.67% for the pure TiO_2 NWs and ~59.15% for the surface-roughened TiO_2 NWs. According to most studies reported previously, the pure TiO_2 prepared at 500 °C consisted of mainly the anatase phase [16]. However, in our study, phase transition from the anatase to the rutile phase may occur because of the presence of the PVP polymer during calcination [16]. In addition, the grain size (D) of the TiO_2 NWs can be calculated using the Scherrer equation [16]:

$$D = 0.9\,\lambda/(\beta \cdot \cos\,\theta)$$

where λ is the X-ray wavelength, β is the full width at half maximum (FWHM), and θ is the Bragg angle. Based on the (101), (110), (101), and (200) planes, the average grain sizes are ~19.72 nm for the pure TiO_2 NWs, and ~18.84 nm for the surface-roughened TiO_2 NWs, which are in good agreement with the TEM results. Although there is little difference in the phase transition and the grain size of the NWs, there is a significant difference between the two samples in the enhanced specific surface area of the surface-roughened TiO_2 NWs. Based on the SEM, TEM, and XRD results, it can be inferred that surface-roughened TiO_2 NWs using co-electrospinning were synthesized successfully.

Fig. 5 displays the photocurrent (J)–voltage (V) curve obtained from the DSSCs fabricated using the pure TiO_2 NWs and the surface-roughened TiO_2 NWs. The measured photovoltaic performances are summarized in Table 1. The open-circuit voltages (V_{oc}) of the two samples show the same value of ~0.67 V, which is because both DSSCs are composed of the TiO_2 NWs as the working electrode and Pt films as the counter electrode. While the fill factor of the samples are almost similar, the short-circuit current densities (J_{sc}) are different, namely, J_{sc} of the surface-roughened TiO_2 NWs (~8.94 mA/cm^2) is greater than that of the pure TiO_2 NWs (~5.88 mA/cm^2). In general, the J_{sc} is strongly related to the dye adsorption on the working electrode [16]. To investigate the amount of dye loading on the TiO_2 NWs, the dye desorption is performed in 0.1 M NaOH solution. It was found that the dye adsorption of the surface-roughened TiO_2 NWs (~1.21×10^{-7} mol/cm^2) is higher than that of the pure TiO_2 NWs (~1.07×10^{-7} mol/cm^2). This result can be explained by the enhanced specific surface area of the surface-roughened TiO_2 NWs, resulting in high production of photo-excited electrons and high J_{sc} in DSSCs, as shown in Table 1 [17,18]. Therefore, the photoconversion efficiency (PCE:η) of the samples was calculated according to the equation given below [15]:

$$\eta(\%) = (J_{sc} \times V_{oc} \times ff)/(P_{in})$$

where J_{sc}, V_{oc}, ff, and P_{in} are the short-circuit photocurrent density, open-circuit voltage, fill factor, and intensity of the incident light (100 mW/cm^2), respectively. The calculated PCE is ~2.36% for the pure TiO_2 NWs and ~3.63% for the surface-roughened TiO_2 NWs, indicating an enhanced PCE of ~34.98%. The performance improvement is attributed to an increase in J_{sc} because of the enhanced dye adsorption, which is due to the increased specific surface area of the TiO_2 NWs induced by the NW shrinkage; this is because of the different thermal decomposition behavior of the PVP depending on their different molecular weights.

Table 1
Summary of the adsorbed amount of dye N719 and photovoltaic performances for DSSCs fabricated with the pure TiO_2 NWs and the surface-roughened TiO_2 NWs.

Samples	Adsorbed dye ($\times 10^{-7}$ mol/cm^2)	V_{oc} (V)	J_{sc} (mA/cm^2)	FF (%)	η (%)
Pure TiO_2NWs	1.07	0.67	5.88	59.23	2.36
Surface-roughened TiO_2NWs	1.21	0.67	8.94	59.89	3.63

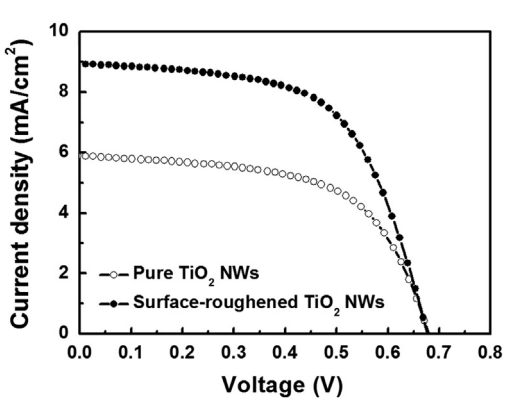

Fig. 5. Photocurrent–voltage (J–V) curves of DSSCs fabricated with the pure TiO_2 NWs and the surface-roughened TiO_2 NWs.

4. Conclusions

The surface-roughened TiO_2 NWs were synthesized using co-electrospinning with different molecular weights of PVP. Together with the formation mechanism of the surface-roughened TiO_2 NWs, the relationship between their structure and photovoltaic performance were demonstrated using TGA, SEM, BET, TEM, XRD, UV–vis spectroscopy, and a solar simulator. Whereas the pure TiO_2 NWs exhibited a dense surface, the surface-roughened TiO_2 NWs had a rough surface. This surface modification can be explained by the NW shrinkage because of the different thermal decomposition behavior of PVP according to their different molecular weights, causing an increase in the specific surface area of

the NWs. Thus, DSSCs fabricated with the surface-roughened TiO_2 NWs showed improved PCE (~3.63%) owing to enhanced J_{sc} because of the improved dye adsorption compared to pure TiO_2 NWs.

Acknowledgment

This work was supported by Grant no. 10046672 from the Ministry of Knowledge Economy (MKE) and R&D Program for Technology of Specialized Materials particularly designed for venture business funded by the Ministry of Knowledge, Republic of Korea.

References

[1] M. Grätzel, Photoelectrochemical cells, Nature 414 (2001) 338–344.
[2] Y. Qiu, W. Chen, S. Yang, Double-layered photoanodes from variable-size anatase TiO_2 nanospindles: a candidate for high-efficiency dye-sensitized solar cells, Angew. Chem. 122 (2010) 3757–3761.
[3] N.-O. Saelim, R. Magaraphan, T. Sreethawong, TiO_2/modified natural clay semiconductor as a potential electrode for natural dye-sensitized solar cell, Ceram. Int. 37 (2011) 659–663.
[4] (a) S.H. Hwang, C. Kim, H. Song, S. Son, J. Jang, Designed architecture of multiscale porous TiO_2 nanofibers for dye-sensitized solar cells photoanode, ACS Appl. Mater. Interfaces 4 (2012) 5287–5292;
(b) M. Zhu, L. Chen, H. Gong, M. Zi, B. Cao, A novel TiO_2 nanorod/nanoparticle composite architecture to improve the performance of dye-sensitized solar cells, Ceram. Int. 40 (2014) 2337–2342.
[5] M. Zhu, L. Chen, H. Gong, M. Zi, B. Cao, A novel TiO_2 nanorod/nanoparticle composite architecture to improve the performance of dye-sensitized solar cells, Ceram. Int. 40 (2014) 2337–2342.
[6] H. Wang, Y. Bai, Q. Wu, W. Zhou, J. Li, L. Guo, Rutile TiO_2 nano-branched arrays on FTO for dye-sensitized solar cells, Phys. Chem. Chem. Phys. 13 (2011) 7008–7013.
[7] T.-S. Kang, A.P. Smith, B.E. Taylor, M.F. Durstock, Fabrication of highly-ordered TiO_2 nanotube arrays and their use in dye-sensitized solar cells, Nano Lett. 9 (2009) 601–606.
[8] H. Hou, L. Wang, G. Wei, J. Chen, W. Yang, B. Tang, F. Gao, Fabrication of TiO_2/SiO_2 hybrid fibers with tunable internal porous structures, Ceram. Int. 40 (2014) 16309–16316.
[9] B.-R. Koo, I.-K. Park, H.-J. Ahn, Fe-doped In_2O_3/α-Fe_2O_3 core/shell nanofibers fabricated by using a co-electrospinning method and its magnetic properties, J. Alloy Compd. 603 (2014) 52–56.
[10] W. Nuansing, S. Ninmuang, W. Jarernboon, S. Maensiri, S. Seraphin, Structural characterization and morphology of electrospun TiO_2 nanofibers, Mater. Sci. Eng. B 131 (2006) 147–155.
[11] M. Chen, H. Qu, J. Zhu, Z. Luo, A. Khasanov, A.S. Kucknoor, N. Haldolaarachchige, D.P. Young, S. Wei, Z. Guo, Magnetic electrospun fluorescent polyvinylpyrrolidone nanocomposite fibers, Polymer 53 (2012) 4501–4511.
[12] M.M. Castillo-Ortega, A.G. Montaño-Figueroa, D.E. Rodríguez-Félix, G. Prado-Villegas, K.P. Pino-Ocaño, M.J. Valencia-Córdova, J.M. Quiroz-Castillo, P.J. Herrera-Franco, Preparation by coaxial electrospinning and characterization of membranes releasing (–) epicatechin as scaffold for tissue engineering, Mater. Sci. Eng. C 46 (2015) 184–189.
[13] X.G. Zhao, J.-Y. Park, H.-B. Gu, Addition of electrospun TiO_2 nanofibers for improving the charge capabilities of polymer electrolyte-based DSSCs, J. Electrochem. Soc. 161 (2014) H517–H522.
[14] D. Chen, F. Huang, Y.-B. Cheng, R.A. Caruso, Mesoporous anatase TiO_2 beads with high surface areas and controllable pore sizes: a superior candidate for high-performance dye-sensitized solar cells, Adv. Mater. 21 (2009) 2206–2210.
[15] G. Li, C.P. Richter, R.L. Milot, L. Cai, C.A. Schmuttenmaer, R.H. Crabtree, G.W. Brudvig, V.S. Batista, Synergistic effect between anatase and rutile TiO_2 nanoparticles in dye-sensitized solar cells, Dalton Trans. (2009) 10078–10085.
[16] W. Wang, M. Gu, Y. Jin, Effect of PVP on the photocatalytic behavior of TiO_2 under sunlight, Mater. Lett. 57 (2003) 3276–3281.
[17] G. Wang, X. Zhu, J. Yu, Bilayer hollow/spindle-like anatase TiO_2 photoanode for high efficiency dye-sensitized solar cells, J. Power Sources 278 (2015) 344–351.
[18] J. Qian, P. Liu, Y. Xiao, Y. Jiang, Y. Cao, X. Ai, H. Yang, TiO_2-coated multilayered SnO_2 hollow microspheres for dye-sensitized solar cells, Adv. Mater. 21 (2009) 3663–3667.